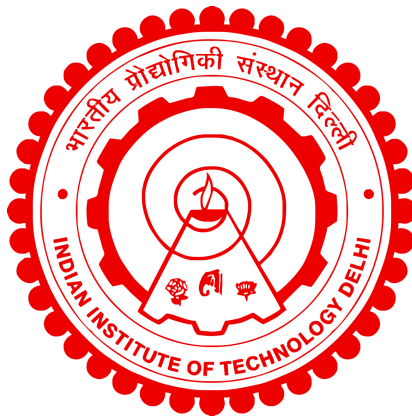


IDENTIFICATION AND BAND ENGINEERING OF NEW TOPOLOGICAL MATERIALS

ANUPAM BHATTACHARYA



DEPARTMENT OF MECHANICAL ENGINEERING

INDIAN INSTITUTE OF TECHNOLOGY DELHI

JULY 2023

©Indian Institute of Technology Delhi (IITD), New Delhi, 2023

**IDENTIFICATION AND BAND
ENGINEERING OF NEW TOPOLOGICAL
MATERIALS**

by

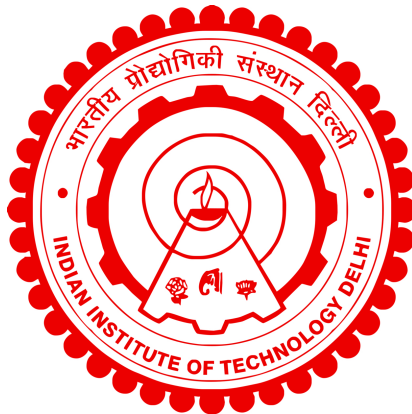
ANUPAM BHATTACHARYA

Department of Mechanical Engineering

Submitted

in partial fulfillment of the requirements of the degree of Doctor of Philosophy

to the



**INDIAN INSTITUTE OF TECHNOLOGY
DELHI**

JULY 2023

§

Dedicated to

...

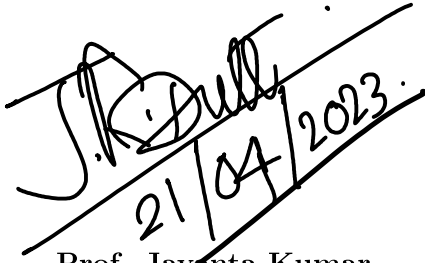
my family

§

Certificate

This is to certify that the thesis entitled “**IDENTIFICATION AND BAND ENGINEERING OF NEW TOPOLOGICAL MATERIALS**”, submitted by **Anupam Bhattacharya** to the Indian Institute of Technology Delhi, for the award of the degree of **Doctor of Philosophy**, is a record of the original, bona fide research work carried out by him under our supervision and guidance. The thesis has reached the standards fulfilling the requirements of the regulations related to the award of the degree.

The results contained in this thesis have not been submitted in part or in full to any other University or Institute for the award of any degree or diploma to the best of our knowledge.



**Prof. Jayanta Kumar
Dutt**

Department of
Mechanical Engineering,
Indian Institute of
Technology Delhi
India



**Prof. Ratnamala
Chatterjee**

Department of Physics,
Indian Institute of
Technology Delhi
India



19/04/2024

**Prof. Artem
Mishchenko**

Department of Physics
and Astronomy,
University of Manchester
United Kingdom

Acknowledgements

With humility in my mind, I take this opportunity to express my gratitude to all those who have contributed to this thesis in various ways.

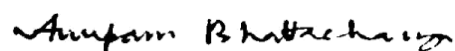
I want to express my deepest gratitude to my supervisors Professor Jayanta Kumar Dutt, Professor Ratnamala Chatterjee, and Professor Artem Mishchenko for their help and support throughout my doctoral study. **Professor Jayanta Kumar Dutt**, with his inquisitive mind and vivid imagination, has always inspired me to think beyond the horizon and has pushed me to realize the thesis as a complete, logical, and cohesive sequence of studies. I shall remain grateful to him for his continued guidance since my Master's study at IIT Delhi, for conveying his crystal-clear view on the philosophy of life to me, and for supporting me at every hurdle and misfortune I faced. I express my heartfelt gratitude to my supervisor **Professor Ratnamala Chatterjee**, who has given me an opportunity to pursue my dream of research in physics while having a background in mechanical engineering. With her confident and encouraging supervision, smart solutions to practical problems, and valuable discussions throughout the work, she has shaped my doctoral thesis to the present form. She granted me the freedom to pursue my research interests and was always available for any help or discussion. I humbly express my sincere gratitude to my supervisor **Professor Artem Mishchenko**, who has shaped my doctoral thesis profoundly in the last two years of my interactions with him. With his vast array of expertise in multiple domains of science, great knowledge of state-of-the-art research topics, and a quick yet effective approach to problems, he has given new dimensions to my doctoral studies. I will remain indebted to him for his continued support even after I left the University of Manchester.

I am grateful to Professor Umesh Waghmare, Theoretical Science Unit, JNCASR, and Professor Brajesh K Mani, Department of Physics, IIT Delhi for teaching me various flavors of theoretical physics and helping with the communicated manuscripts. I feel lucky to have worked with such illustrious physicists. I would like to thank my Student Research Committee (SRC) members Professor Anoop Chawla, Professor Satinder Paul Singh, and Dr. Sushma Santapuri for their valuable suggestions during the course of this work.

I would like to acknowledge the IIT Delhi HPC facility for computational resources. During my doctoral study, I visited the University of Manchester, UK the Commonwealth scholarship. I sincerely thank the University and its staff for hosting me and Commonwealth Scholarship Commission in the UK for financial support. I further acknowledge MHRD India and IIT Delhi for their financial support throughout my study.

I thank all my colleagues at IIT Delhi, Dr. Parul, Dr. Sandeep Kumar, Dr. Vishal Bhardwaj, Dr. Divyanshu Bhatnagar, Dr. Deepika Dabra, Dr. Mithun Majee, Dr. Devendra Dubey, Dr. Satyendra Parkash Pal, Dr. Thirumal, Vikas Malik, Divya Prakash Dubey, Hitesh Gulati, Priyanka Sharma, Durgesh Ojha, Shivangi Srivastava, Pankaj Kumar, Vikas Chahar, Balwant Chauhan, Anshul Toshniwal, Saheen Alam, Md. Shadab Anwar and Ganga Prasad (Rinku) for their cooperation and support. I sincerely thank Dr. Qian Yang, Dr. Ivan Timokhin, Dr. Pablo Díaz Núñez, Dr. Sergey Slizovskiy, Megjie Feng, Ziwei Wang, and Ciaran Mullan from the University of Manchester for their help and support during my study.

Finally, I would like to express my love and gratefulness to the members of the unique family of mine, which is without a doubt the most loving, caring, and supportive one that I have ever seen. If rebirth was indeed possible, I would like to be born again in the same family. Thank you!



Anupam Bhattacharya

New Delhi
18 April 2023

...

Abstract

TOPOLOGY, an esoteric branch of mathematics, studies different classes of objects which have fundamentally similar geometrical structures. Objects within each of these classes can be continuously deformed to create each other. Topology has acquired its strong foothold in the domain of solid-state physics and materials science, with its application to explain the integer quantum Hall effect in the late twentieth century. Since then, topological properties were associated with the electronic and phononic structures of various materials. In this thesis, only electronic topological properties were studied, and therefore, the phrase ‘topological materials’ will be used to refer to materials with topologically distinct electronic structures. These materials show geometrically protected knots in their electronic structures owing to their special lattice structure and constituent elements. These topological knots are immune to small perturbations and defects in the materials and thus, the properties of these materials are robust as long as the underlying reason behind the topological knot is not destroyed. These materials can be of several types based on their nature of electronic dispersion. Topological materials which have band openings at the Fermi level are classified into topological insulators and topological crystalline insulators respectively depending on the absence or existence of any spatial symmetry protecting the non-triviality. When topological materials have metallic energy vs. momenta ($E - k$) dispersion, they are called topological metals. These metals can be of several types, viz. Weyl, Dirac, triple-point, and nodal line semimetals based on the dimensionality and number of degenerate states at the topologically protected crossings. Topological flat band materials are another kind of these materials that show no dispersion of certain electronic states owing to destructive interference of Bloch wavefunctions.

In the last few decades, the study of topology in solid-state materials has found numerous applications to bring this subject to the limelight of research interests. Topological materials were found to be a possible pathway to realize qubits for next-generation quantum computers. Topological insulators and metals have emerged as promising candidates for new generations of transistors and processors. Also, these materials have found applications in spin-based electronics or spintronics. Topological insulators, metals, and flat-band materials have been shown to give rise to a new

type of superconductivity or topological superconductivity. In this thesis, artificial intelligence, first-principle methods, and $k.p$ perturbation theory have been utilized to identify new topological flat-band materials and pathways to engineer topological transitions among different topological metallic states. In the first chapter, the objectives of the thesis are introduced and a literature review on relevant topological materials is presented. In the second chapter, the basics of the theoretical methods used in the thesis are described. The subsequent chapters describe the work done to achieve the objectives.

In the third chapter of the thesis, the origin of topological flat bands was studied using a data-driven approach. A deep neural network was utilized to identify flat bands within the band structures of materials (from a 2D-materials database for tractable size). The materials thus identified are further categorized based on the coordination of the atom by which the flat band is populated. This categorization leads to the identification of 48 lattice geometries responsible for flat dispersion, many of which have been identified in recent literature. Therefore, the present study generates a database of all possible 2D lattice structures that can lead to flat bands, helping focused research on newly identified lattice structures as a future scope. Although this study started with a goal of identifying only topological flat band materials, it ended up with a database of all flat band materials of which the former is a subset. This is because the state of the art in this domain does not have the means (utilizing only $E - k$ dispersion data) to separate topological non-trivial band structures from their trivial counterparts as of yet. It may be performed with help of charge density data or electronic wavefunction data, but open databases usually do not host these data due to storage constraints. Thus, the task of isolating the topologically nontrivial bands from flat bands remains a future scope.

In the next two chapters, engineering approaches to manipulate electronic bands of newly discovered topological materials to witness topological transitions are studied. Towards this, the use of mechanical strain in cases of nonmagnetic materials and magnetic fields/spin-torques in cases of magnetic materials were explored. The fourth chapter focuses on the use of strain to attain topological transition in the diamagnetic RE-PdBi ('RE' refers to Rare-Earth) series. YPdBi, a diamagnetic RE-half Heusler alloy, lying near the boundary between trivial and non-trivial materials was studied first to show a transition to the non-trivial state under tensile strain. To

validate the theoretical observation with experiments, a semi-infinite slab is modeled to replicate the behavior of thin films. Simulations with the slab show the existence of surface-originated high-mobility electrons near Fermi energy in agreement with the experiments. The experiments also show signatures of topological non-triviality as demonstrated by the theory. Inspired by the study on YPdBi, other diamagnetic half-Heusler alloys were studied under tensile and compressive strain. It was found that the topological triple-point semimetallic state of these metals evolves under strain changing the number of triple-point nodes. It was also found that these transitions are accompanied by multiple band-inversions near Fermi energy. A phase diagram for ease of material selection is presented.

In the fifth chapter, topological transitions were studied under a magnetic field or spin torque. DyPdBi, an antiferromagnetic half-Heusler alloy was chosen for the study, which lies near the boundary between trivial and non-trivial materials. It was found that DyPdBi can show a transition between two topological semimetallic states. When the local magnetic moments of dysprosium are oriented to the three-fold rotation C_3 axis of the crystal, i.e. when the C_{3v} symmetry is preserved, DyPdBi hosts four topological nodes along the C_3 axis of the Brillouin zone, making it a triple-point semimetal. When the local magnetic moments of Dy are oriented to a direction perpendicular to the three-fold rotational axis, the antiferromagnetic structure has four Weyl nodes, two on each side of the mirror plane of its Brillouin zone. The triple point fermions of DyPdBi give rise to a characteristic peak in the anomalous Hall conductivity response, but the Weyl fermions can not contribute to the anomalous Hall conductivity response. The difference in energy between these two topologically distinct states is a mere ≈ 15 meV, making them switchable with a magnetic field or spin torque.

In the final chapter, the conclusions of the research work are explained in brief. The scope of future research work is also described in this chapter. In a nutshell, there are several novel impactful outcomes of the research conducted in the thesis.

- The deep learning-assisted study described in the third chapter yields a family of AI-based tools readily applicable to any materials database to identify flat-band generating sublattices, many of which are potentially topologically

nontrivial. This will help identify new functional materials potentially hosting highly correlated physics like unconventional superconductivity.

- The study on strain-based topological transition gives us pathways to choose the appropriate material and stress required for fine-tuning bulk and surface transport characteristics by utilizing the topological phase diagram of diamagnetic RE-half Heusler alloys.
- The study on magnetic field-driven topological transitions gives a way to distinguish Weyl and triple point metallic phases experimentally through signatures in anomalous Hall conductance.

संस्थितिविज्ञान, गणित की एक गूढ़ शाखा है, वस्तुओं के विभिन्न वर्गों का अध्ययन करती है जिनमें मौलिक रूप से समान ज्यामितीय संरचनाएं होती हैं। इनमें से प्रत्येक वर्ग के भीतर वस्तुओं को एक दूसरे को बनाने के लिए लगातार विकृत किया जा सकता है। संस्थितिविज्ञान ने बीसवीं शताब्दी के अंत में पूर्णांक क्वांटम हॉल प्रभाव की व्याख्या करने के लिए अपने आवेदन के साथ, ठोस-राज्य भौतिकी और सामग्री विज्ञान के क्षेत्र में अपनी मजबूत पकड़ हासिल कर ली है। तब से, टोपोलॉजिकल गुण विभिन्न सामग्रियों के इलेक्ट्रॉनिक और ध्वन्यात्मक संरचनाओं से जुड़े थे। इस निबंध में, केवल इलेक्ट्रॉनिक टोपोलॉजिकल गुणों का अध्ययन किया गया था, और इसलिए, टोपोलॉजिकल रूप से अलग-अलग इलेक्ट्रॉनिक संरचनाओं के साथ सामग्री को संदर्भित करने के लिए 'टोपोलॉजिकल सामग्री' वाक्यांश का उपयोग किया जाएगा। ये सामग्री अपनी विशेष जाली संरचना और घटक तत्वों के कारण अपनी इलेक्ट्रॉनिक संरचनाओं में ज्यामितीय रूप से संरक्षित गाँठें दिखाती हैं। ये टोपोलॉजिकल गाँठें सामग्री में छोटे गड़बड़ी और दोषों से प्रतिरक्षित हैं और इस प्रकार, इन सामग्रियों के गुण तब तक मजबूत होते हैं जब तक कि टोपोलॉजिकल गाँठ के पीछे अंतर्निहित कारण नष्ट नहीं हो जाते। इलेक्ट्रॉनिक फैलाव की प्रकृति के आधार पर ये सामग्रियां कई प्रकार की हो सकती हैं। गैर-तुच्छता की रक्षा करने वाले किसी भी स्थानिक समरूपता की अनुपस्थिति या अस्तित्व के आधार पर टोपोलॉजिकल सामग्री जिसमें फर्मी स्तर पर बैंड के उद्घाटन होते हैं, उन्हें क्रमशः टोपोलॉजिकल इंसुलेटर और टोपोलॉजिकल क्रिस्टलीय इंसुलेटर में वर्गीकृत किया जाता है। जब टोपोलॉजिकल सामग्री में धात्विक ऊर्जा बनाम संवेग ($E-k$) फैलाव होता है, तो उन्हें टोपोलॉजिकल धातु कहा जाता है। ये धातुएँ कई प्रकार की हो सकती हैं, जैसे। वेइल, डिराक, ट्रिपल-पॉइंट, और नोडल लाइन सेमी-मेटल्स, आयामी रूप से संरक्षित क्रॉसिंग पर आयामीता और पतित अवस्थाओं की संख्या के आधार पर। टोपोलॉजिकल फ्लैट बैंड सामग्री एक अन्य प्रकार की सामग्री है जो बलोच वेवफंक्शन के विनाशकारी हस्तक्षेप के कारण कुछ इलेक्ट्रॉनिक राज्यों का फैलाव नहीं दिखाती है।

पिछले कुछ दशकों में, ठोस-राज्य सामग्री में टोपोलॉजी के अध्ययन ने इस विषय को अनुसंधान के हितों की सुर्खियों में लाने के लिए कई अनुप्रयोग पाए हैं। अगली पीढ़ी के क्वांटम कंप्यूटरों के लिए qubits को साकार करने के लिए टोपोलॉजिकल सामग्रियों को एक संभावित मार्ग के रूप में पाया गया। टोपोलॉजिकल इंसुलेटर और धातु ट्रांजिस्टर और प्रोसेसर की नई पीढ़ी के लिए आशाजनक उम्मीदवार के रूप में उभरे हैं। साथ ही, इन सामग्रियों को स्पिन-आधारित इलेक्ट्रॉनिक्स या स्पिट्रॉनिक्स में अनुप्रयोग मिला है। टोपोलॉजिकल इंसुलेटर, धातु और फ्लैट-बैंड सामग्री को एक नए प्रकार की सुपरकंडक्टिविटी या टोपोलॉजिकल सुपरकंडक्टिविटी को जन्म देने के लिए दिखाया गया है। इस थीसिस में, आर्टिफिशियल इंटेलिजेंस, प्रथम-सिद्धांत विधियों और $k.p$ पर्टर्बेशन थ्योरी का उपयोग नए टोपोलॉजिकल फ्लैट-बैंड सामग्रियों की पहचान करने और विभिन्न टोपोलॉजिकल मेटालिक स्टेट्स के बीच इंजीनियर टोपोलॉजिकल ट्रांजिशन के लिए किया गया है। पहले अध्याय में, थीसिस के उद्देश्यों को पेश किया गया है और प्रासंगिक सामयिक सामग्री पर एक साहित्य समीक्षा प्रस्तुत की गई है। द्वितीय अध्याय में शोध प्रबंध में प्रयुक्त

सैद्धान्तिक विधियों के मूल सिद्धांतों का वर्णन किया गया है। बाद के अध्याय उद्देश्यों को प्राप्त करने के लिए किए गए कार्यों का वर्णन करते हैं।

शोध प्रबंध के तीसरे अध्याय में, डेटा-चालित दृष्टिकोण का उपयोग करके टोपोलॉजिकल फ्लैट बैंड की उत्पत्ति का अध्ययन किया गया था। सामग्री के बैंड संरचनाओं के भीतर फ्लैट बैंड की पहचान करने के लिए एक गहरे तंत्रिका नेटवर्क का उपयोग किया गया था (ट्रैक्टेबल आकार के लिए 2डी-सामग्री डेटाबेस से)। इस प्रकार पहचानी गई सामग्रियों को परमाणु के समन्वय के आधार पर आगे वर्गीकृत किया जाता है जिसके द्वारा फ्लैट बैंड आबाद होता है। यह वर्गीकरण फ्लैट फैलाव के लिए जिम्मेदार 48 जाली ज्यामिति की पहचान की ओर जाता है, जिनमें से कई की पहचान हाल के साहित्य में की गई है। इसलिए, वर्तमान अध्ययन सभी संभव 2डी जाली संरचनाओं का एक डेटाबेस उत्पन्न करता है जो भविष्य के दायरे के रूप में नई पहचानी गई जाली संरचनाओं पर केंद्रित शोध में मदद करते हुए फ्लैट बैंड का कारण बन सकता है। हालांकि यह अध्ययन केवल टोपोलॉजिकल फ्लैट बैंड सामग्रियों की पहचान करने के लक्ष्य के साथ शुरू हुआ, यह सभी फ्लैट बैंड सामग्रियों के डेटाबेस के साथ समाप्त हुआ, जिनमें से पूर्व एक सबसेट है। ऐसा इसलिए है क्योंकि इस डोमेन में कला की स्थिति में उनके तुच्छ समकक्षों से टोपोलॉजिकल गैर-तुच्छ बैंड संरचनाओं को अलग करने के लिए साधन (केवल ऊर्जा बनाम संवेग डेटा का उपयोग) नहीं है। यह चार्ज घनत्व डेटा या इलेक्ट्रॉनिक वेवफंक्शन डेटा की मदद से किया जा सकता है, लेकिन खुले डेटाबेस आमतौर पर भंडारण की कमी के कारण इन डेटा को होस्ट नहीं करते हैं। इस प्रकार, फ्लैट बैंड से स्थैतिक रूप से गैर-तुच्छ बैंड को अलग करने का कार्य भविष्य का दायरा बना हुआ है।

अगले दो अध्यायों में, टोपोलॉजिकल ट्रांज़िशन देखने के लिए नए खोजे गए टोपोलॉजिकल सामग्रियों के इलेक्ट्रॉनिक बैंड में हेरफेर करने के लिए इंजीनियरिंग दृष्टिकोण का अध्ययन किया गया है। इसके लिए, गैर-चुंबकीय सामग्री के मामले में यांत्रिक तनाव और चुंबकीय सामग्री के मामले में चुंबकीय क्षेत्र/स्पिन-टोर्क का पता लगाया गया। चौथा अध्याय प्रतिचुंबकीय आरई-पीडीबीआई (‘आरई’ दुर्लभ-पृथ्वी को संदर्भित करता है) श्रृंखला में सामयिक संक्रमण प्राप्त करने के लिए तनाव के उपयोग पर केंद्रित है। YPdBi, एक डायनामैग्नेटिक आरई-हाफ हेस्लर मिश्र धातु, तुच्छ और गैर-तुच्छ सामग्रियों के बीच की सीमा के पास स्थित है, पहले तन्य तनाव के तहत गैर-तुच्छ अवस्था में संक्रमण दिखाने के लिए अध्ययन किया गया था। प्रयोगों के साथ सैद्धान्तिक अवलोकन को मान्य करने के लिए, पतली फिल्मों के व्यवहार को दोहराने के लिए एक अर्ध-अनंत स्लैब तैयार किया गया है। स्लैब के साथ सिमुलेशन प्रयोगों के साथ समझौते में फर्मी ऊर्जा के पास सतह से उत्पन्न उच्च-गतिशीलता वाले इलेक्ट्रॉनों के अस्तित्व को दर्शाता है। प्रयोग सिद्धांत द्वारा प्रदर्शित के रूप में स्थलीय गैर-तुच्छता के हस्ताक्षर भी दिखाते हैं। YPdBi पर अध्ययन से प्रेरित होकर, अन्य प्रतिचुंबकीय अर्ध-हेस्लर मिश्रधातुओं का अध्ययन तन्यता और संपीडन तनाव के तहत किया गया। यह पाया गया कि इन धातुओं की टोपोलॉजिकल ट्रिपल-पॉइंट सेमीमेटेलिक स्थिति ट्रिपल-पॉइंट नोड्स की संख्या को बदलते हुए तनाव के तहत विकसित होती है। यह भी पाया गया कि ये संक्रमण फर्मी ऊर्जा के पास कई बैंड-इनवर्जन के साथ हैं। सामग्री चयन में आसानी के लिए एक चरण आरेख प्रस्तुत किया गया है।

पांचवें अध्याय में, एक चुंबकीय क्षेत्र या स्पिन टॉर्क के तहत टोपोलॉजिकल ट्रांज़िशन का अध्ययन किया गया था। DyPdBi, एक एंटीफेरोमैग्नेटिक हाफ-हेस्लर मिश्र धातु को अध्ययन के लिए चुना गया था, जो तुच्छ और गैर-तुच्छ सामग्रियों के बीच की सीमा के पास स्थित है। यह पाया गया कि DyPdBi दो टोपोलॉजिकल सेमीमेटलिक अवस्थाओं के बीच संक्रमण दिखा सकता है। जब डिस्प्रेसियम के स्थानीय चुंबकीय क्षण क्रिस्टल के तीन गुना रोटेशन C_3 अक्ष के लिए उन्मुख होते हैं, यानी जब C_{3v} समरूपता संरक्षित होती है, तो DyPdBi ब्रिल्लिन ज़ोन के C_3 अक्ष के साथ चार टोपोलॉजिकल नोड्स होस्ट करता है, जिससे यह एक ट्रिपल बन जाता है -पॉइंट सेमीमेटल। जब डाई के स्थानीय चुंबकीय क्षण तीन गुना घूर्णी अक्ष के लंबवत दिशा में उन्मुख होते हैं, तो एंटीफेरोमैग्नेटिक संरचना में चार वेइल नोड होते हैं, दो इसके ब्रिलॉइन ज़ोन के दर्पण तल के प्रत्येक तरफ होते हैं। DyPdBi के ट्रिपल पॉइंट फ़र्मियन विषम हॉल चालकता प्रतिक्रिया में एक विशिष्ट शिखर को जन्म देते हैं, लेकिन वीइल फ़र्मियन विषम हॉल चालकता प्रतिक्रिया में योगदान नहीं कर सकते हैं। इन दो स्थैतिक रूप से भिन्न अवस्थाओं के बीच ऊर्जा का अंतर लगभग 15 meV है, जो उन्हें चुंबकीय क्षेत्र या स्पिन टॉर्क के साथ स्विच करने योग्य बनाता है।

अन्तिम अध्याय में शोध कार्य के निष्कर्षों का संक्षेप में वर्णन किया गया है। इस अध्याय में भावी शोध कार्य के क्षेत्र का भी वर्णन किया गया है।

संक्षेप में, थीसिस में किए गए शोध के कई उपन्यास प्रभावशाली परिणाम हैं।

- तीसरे अध्याय में वर्णित गहन शिक्षण-सहायता अध्ययन से फ्लैट-बैंड जनरेटिंग सबलैटिस की पहचान करने के लिए किसी भी सामग्री डेटाबेस पर आसानी से लागू होने वाले एआई-आधारित उपकरणों का एक परिवार मिलता है, जिनमें से कई संभावित रूप से गैर-तुच्छ हैं। यह अपरंपरागत सुपरकंडक्टिविटी जैसे अत्यधिक सहसंबद्ध भौतिकी की मेजबानी करने वाली नई कार्यात्मक सामग्रियों की पहचान करने में मदद करेगा।
- स्ट्रेन-आधारित टोपोलॉजिकल ट्रांज़िशन पर अध्ययन हमें डायनामैग्नेटिक आरई-हाफ हेस्लर मिश्र धातुओं के टोपोलॉजिकल चरण आरेख का उपयोग करके बल्क और सतह परिवहन विशेषताओं को ठीक करने के लिए आवश्यक उपयुक्त सामग्री और तनाव का चयन करने के लिए मार्ग प्रदान करता है।
- चुंबकीय क्षेत्र-संचालित टोपोलॉजिकल ट्रांज़िशन पर अध्ययन विषम हॉल चालन में हस्ताक्षर के माध्यम से प्रयोगात्मक रूप से वेइल और ट्रिपल बिंदु धातु चरणों को अलग करने का एक तरीका देता है।

Contents

Certificate	i
Acknowledgements	ii
Abstract	iv
Contents	xi
List of Figures	xv
List of Tables	xxi
Abbreviations	xxiii
1 Introduction	1
1.1 Topological invariance	3
1.1.1 Homomorphism and isomorphism	3
1.1.2 Homeomorphism	4
1.1.3 Euler characteristic and genus	5
1.1.4 Topological invariants of electronic states	7
1.2 Topological features in electronic bands	12
1.2.1 Topological insulators	13
1.2.1.1 2D topological insulators	14
1.2.1.2 3D topological insulators	16
1.2.2 Topological crystalline insulators	16
1.2.3 Topological metals and semimetals	17
1.2.3.1 Weyl metals	18
1.2.3.2 Dirac metals	20
1.2.3.3 Three (triple point) and higher fold topological metals	21
1.2.3.4 Nodal line metals	22

1.2.3.5	Types of dispersion in topological metals	23
1.2.3.6	Invariants of topological metals	25
1.2.4	Topological flatband materials	26
1.3	Application of topological states of materials	27
1.4	Background and Motivation	31
1.4.1	Role of open databases in identifying topological materials	31
1.4.2	Rare-earth half-Heusler alloys: a host of multiple topological phases	35
1.5	Thesis Organisation	42
2	Theoretical background	47
2.1	Artificial intelligence in materials science	47
2.2	First principle methods	50
2.2.1	Schrödinger Equation	51
2.2.2	Early first-principle methods	53
2.2.2.1	Hartree method	54
2.2.2.2	Hartree-Fock method	55
2.2.3	Density functional theory	55
2.2.3.1	Hohenberg-Kohn theorems	56
2.2.3.2	Kohn-Sham formulation of the energy terms	58
2.2.3.3	Kohn-Sham equation	63
2.2.3.4	Solving the Kohn-Sham equation	64
2.3	$k.p$ perturbation theory	66
3	Identification of flat band lattices using deep learning from open databases	69
3.1	Architecture of the algorithm for identifying flat band lattices	72
3.1.1	Identification of flat bands using CNN	72
3.1.2	Identification of flat band sublattices	74
3.1.3	Unsupervised machine learning: bilayer clustering	76
3.1.4	Evolution of the identified coordination patterns and lattice structures	79
3.2	Details of the identified lattice structures	82
3.2.1	Finer search for recurrent lattice structures	87
3.3	Discussions	91
3.4	Further details of the methods used	93
3.4.1	Convolutional neural network	93
3.4.2	Sublattice extraction and vectorization	95
3.4.3	Clustering module	98
3.4.4	Visualization of flat band clusters using UMAP	99
3.4.5	Validity of sublattice selection	100
3.4.6	Distribution of sublattice elements	102

3.4.7	Use of SOAP descriptor in clustering algorithm	104
4	Topology switching in Diamagnetic RE Half Heusler alloys using strain	107
4.1	Topological non-triviality of strained YPdBi thin films	108
4.2	Topological non-triviality in diamagnetic bulk RE-half Heusler alloys	112
4.2.1	Tensile strain induced band-inversion in diamagnetic RE half Heusler alloys	113
4.2.2	Band inversion mechanism in diamagnetic RE-PdBi	115
4.2.3	Triple point semi-metallicity	118
4.2.4	Surface electronic structure	122
4.2.5	Band inversion and triple points in ScPdBi and LaPdBi through tensile strain	124
4.2.6	Band inversion and triple points in YPtBi, LuPtBi and LuPdBi through compressive strain	126
4.2.7	HSE06 band-structures	127
4.2.8	Discussion	129
4.3	Details of first-principle calculations	131
5	Topology switching in antiferromagnetic RE Half Heusler alloys using magnetic field	133
5.1	Crystal structure of DyPdBi	136
5.2	Electronic structure of AFM- state of DyPdBi with magnetic moments along [111]	137
5.2.1	Electronic band dispersion and topological nodal points	137
5.2.2	Surface electronic structure and topological fermi arcs	140
5.3	Electronic structure of AFM- \perp state of DyPdBi with magnetic moments perpendicular to [111]	141
5.3.1	Band-dispersion and topologically protected crossings	142
5.3.2	Surface electronic structure and topological Fermi arcs	146
5.4	Characteristic difference between Weyl and triple point Fermions identified through AHC	146
5.5	Details of first-principles calculations	150
6	Conclusions and outlook	153
6.1	Conclusions from deep learning assisted identification of flat band lattices	153
6.2	Conclusions from the study on YPdBi thin films	154
6.3	Conclusions from the study on topological transition in diamagnetic RE-half Heusler alloys	154
6.4	Conclusions from the study on topological transition in AFM RE-half Heusler alloys	155
6.5	Contributions to the state of the art	155

6.6	Scope for future research	156
A	Mechanical, thermodynamic and lattice dynamical properties of RE-PdBi	157
A.1	Introduction	157
A.2	Results and discussions	159
A.2.1	Calculation of accurate lattice parameters	159
A.2.2	Single crystal elastic moduli	161
A.2.2.1	Anisotropy of single crystalline elastic constants	165
A.2.3	Polycrystalline estimates of elastic moduli	166
A.2.3.1	VRH approximation	166
A.2.3.2	Ductility	170
A.2.4	Thermodynamic properties and experimental validation	171
A.2.4.1	Speed of sound	171
A.2.4.2	Debye temperature	173
A.3	Summary	173
A.4	Details of first principle calculations	175
B	Symmetry analysis of antiferromagnetic RE-PdBi alloys	177
B.1	Group theoretical study of DyPdBi	177
B.1.1	8×8 Hamiltonian	178
B.1.2	Löwdin partitioning	180
B.1.3	AFM- \parallel phase	181
B.1.4	AFM- \perp phase	183
B.2	Symmetry analysis of AHC in RE-PdBi	185
C	Fermi arc connectivity among topological nodes in antiferromagnetic RE-PdBi	189
C.1	Connectivity among triple points	190
C.2	Connectivity among the Weyl points	191
D	Magnetocrystalline anisotropy in antiferromagnetic RE-PdBi	195
D.1	Lattice structures	196
D.2	Self-consistent calculation of Hubbard U parameter	196
D.3	Calculation of anisotropy energies	197
D.4	Details of the first principles calculations	199
	Bibliography	201
	List of publications from this thesis	237
	Bio-data	239

List of Figures

1.1	Homeomorphism f maps two 1D manifolds G and H	5
1.2	(a) 2D polygon with $\chi = 1$. (b) 3D polyhedra with $\chi = 2$. (c) Examples of orientable surfaces with $\chi = 0$, (d) some non-orientable surfaces.	6
1.3	Electronic band inversion in topologically nontrivial HgTe (left) compared to its trivial counterpart CdTe (right). Adapted from [8].	15
1.4	Typical electronic dispersion around Dirac (a) and Weyl (b) points. Adopted from [24].	18
1.5	Typical electronic dispersion around a nodal line semimetal (a) and triple point semimetal(b). Adopted from [25].	23
1.6	Electronic dispersion and configuration of electron-hole pockets around (a) type-I (b) type-II and (c) type-III point node semimetals. Adopted from [46].	24
1.7	Calculation of topological invariants for topological metals. Adopted from [23].	25
1.8	Tunnelling probability among localized states differentiates trivial flat bands from their nontrivial counterparts. Adopted from [50].	26
1.9	(a) Lattice structure of half-Heusler alloys. (b) Constituent elements of half-Heusler alloys are shown in matching colors with the left panel. Image courtesy: Bai et. al[87].	35
1.10	(a-h) s-like character of bands at Γ point bleeds into valence bands below Fermi energy showing inversion of orbital character. (b) Rare-earth half-Heusler materials with predicted trivial and non-trivial band topology. Image courtesy: Sawai et al.[91], Chadov et al. [92].	36
1.11	(a-b) Topology engineering in rare-earth half Heusler alloys using strain. (c) Tuning anomalous Hall effect in GdPtBi using pressure. Image courtesy: Lin et al. [93], Sawai et al.[91], Sun et al. [98].	38
2.1	Paradigms of scientific discovery (adapted from [108]).	48
2.2	Flowchart of the self-consistent algorithm used in DFT.	65

- 3.1 Architecture of combined supervised and unsupervised machine learning algorithms used in this work. CNN was trained to identify flat band materials using segmented band structure images from the database, followed by identifying sublattices that are responsible for flat dispersion using element projected DOS. Then, density-based clustering combined with t-SNE was used to classify the assigned structural fingerprints, and to identify classes of flat band 2D materials. 73
- 3.2 Identification of flat bands from band structure images using supervised machine learning. (a) Segmentation of band structure images from 2Dmatpedia, and identification of flat band segments. Left panel: segmentation of band structure image of SnCl_4 [2dm-13] horizontally into four 0.5 eV energy strips, and vertically along high symmetry points in k-space, as denoted in green, blue, and yellow for $\Gamma \rightarrow X$, $X \rightarrow M$, and $M \rightarrow \Gamma$ paths, respectively. Right panel: segmented band structure in the [-1,1] eV range and predicted outputs. Segments with flat bands are marked in red frames their corresponding flatness score is shown on top. (c) Histogram of compound flatness scores of all the materials in 2Dmatpedia. 74
- 3.3 Identification of flat band sublattices. (a) Band structure of an identified flat band material example $\text{Pd}_3\text{P}_2\text{S}_8$. (b) Element projected DOS from (a) reveals the element responsible for flat band is Pd. (c) The crystal structure of $\text{Pd}_3\text{P}_2\text{S}_8$. (d) Kagome sublattice of Pd remains after stripping off P and S elements from $\text{Pd}_3\text{P}_2\text{S}_8$ structure. 75
- 3.4 HDBSCAN algorithm optimization. Graphs showing (a) DBCV index, (b) S_Dbw indices, (c) number of clusters and (d) number of unclassified materials as functions of minimum cluster size (MS) and sample size for density calculation (SS). 78
- 3.5 Clustering solution from HDBSCAN with $MS = 7$, $SS = 6$. (a) Phylogenetic tree expression of the hierarchical relations among clusters represented by colored circles. The size of each circle is proportional to the corresponding cluster's volume, while the cluster index is indicated by the number nearby. (b) t-SNE 2D visualization of the structure fingerprint space, different coordination patterns are color-coded; ip is in-plane and oop is out-of-plane coordination. Insets are representative coordination templates, where atoms in different atomic planes of the templates are colored differently. 80
- 3.6 Clustering results from HDBSCAN for $MS=4$, $SS=3$. (a) Condensed tree plot showing hierarchical information among clusters with numbers representing cluster IDs. (b) t-SNE plot showing adjacency of materials in the embedded space. Numbers represent cluster IDs. . . 88

3.7	(a) Number of flat bands identified in each energy bandwidth. The sum of these numbers surpass the total of 2127 flat band materials identified from 5270 materials in 2dmatpedia. This is because some materials have multiple flat bands at different energy segments within the ± 1 eV of Fermi energy. (b) Priority assignment for each energy segment in the cases where more than one flat band is identified in the same material across multiple energy segments.	97
3.8	Optimized UMAP visualization (Nearest_neighbor = 30) for HDBSCAN output of MS=7 and SS=6.	99
3.9	(a) Histogram of sublattice scores of flat band materials identified from 2Dmatpedia. (b) Colormap of the primary sublattice score S_1 for each flat band material of 2Dmatpedia shown in t-SNE plot. . . .	101
3.10	Percentage of the elements responsible for flat band sublattices shown as a colormap on the periodic table.	103
3.11	Colormap of elements showing a tendency to form flat electronic bands. Color scale shows the ratio R of the number of compounds with a flat band from an element sublattice to the total number of appearances for this element in the database.	103
3.12	t-SNE visualization of HDBSCAN Clustering with SOAP fingerprints with Gaussian $\sigma = 1\text{\AA}$. (a) Panel shows the full embedded space without annotations (b) Zoomed embedded space annotating cluster IDs in the same colors as the clusters.	105
4.1	(a) Primitive unit cell of YPdBi with its (b) first Brillouin zone. (c) Minimum energy lattice parameter calculated for YPdBi. (d) Unstrained band structure of YPdBi. (e) Band structure of YPdBi under 3.12% strain.	110
4.2	(a) Semi-infinite slab of YPdBi consisting of 8 unit cell layers and (b) its 2D Brillouin zone. (c) Electronic pockets formed by two valence bands. (d-f) Electronic dispersion curve of YPdBi slab made of 8, 14 and 20 unit cell layers.	111
4.3	(a-i) Band structure in YPdBi, ScPdBi and LaPdBi as a function of uniform tensile strain. Similar data for LuPdBi, YPtBi and LuPtBi under compressive strain are presented in the supplementary information.	114
4.4	Electronic band-structure of YPdBi under uniform tensile strain showing two band inversions. Dark green and light green colors represent s type and p type bands respectively.	116
4.5	(a) Change in Fermi energy, Γ_6 , Γ_8 and Γ_7 with tensile strain. (b) Change in electronic occupation from unstrained state.	117

4.6	Triple points (marked with red circles) in YPdBi at (a) 2%, (b) 4% and (c) 5% tensile strain. (d) Trajectories of triple points in diamagnetic half-Huesler alloys as function of RBIS. The red, magenta and blue lines represent the trajectories of the outer-most, middle and inner-most triple points respectively.	119
4.7	Electronic structure of semi-infinite slabs of YPdBi under (a) 2% (b) 4% and (c) 5% tensile strains. Inset in (a) shows 2D BZ of the semi-infinite slab with high symmetry points.	123
4.8	(a-e) Band inversions and triple points in ScPdBi under tensile strain. (c,e) The zoomed view of triple points around Γ point in ScPdBi. (f-h) Band inversions and triple points in LaPdBi under tensile strain.	125
4.9	Band inversions and triple points in LuPdBi (a-e), YPtBi (f-i) and LuPtBi (j-m) under compressive strains.	127
4.10	(a) The change in Fermi energy and the energies of Γ_6 , Γ_8 and Γ_7 with compressive strain in LuPdBi. (b) The change in the occupation of various orbitals with compressive strain.	128
4.11	HSE bandstructure using GGA optimized lattice parameters for YPdBi (a), ScPdBi (b) and LaPdBi (c).	128
4.12	HSE bandstructure using experimental lattice parameters for YPdBi (a), ScPdBi (b) and LaPdBi (c).	129
5.1	Primitive unit cell of DyPdBi in crystal structure with symmetry of space group R3m and antiferromagnetically ordered spins of Dy along the C_3 axis (AFM-) (a), its Electronic structure (b) calculated with inclusion of the SOC, corresponding Brillouin zone (c) with high symmetry k-points, and locations of the triple point nodes in the BZ (d).	135
5.2	Total and orbital projected band structure along $Z - \Gamma - Z'$ showing contributions of (a) s, p and d orbitals, (b) spin-orbit split bands constituted of p -orbitals of Bi (top panels) and of d -orbitals of Dy (bottom panels). These results have been obtained with kresolved_dos module of the QE package.	136
5.3	Electronic structure of Dy-terminated (100) surface of AFM- DyPdBi calculated using Wannier functions based tight-binding model with Wannier90 and WannierTools packages, displayed as contourplots of k-resolved density of states (a) in which the nodal points and conical band structural features at 0.006 eV and -0.013 eV are marked by dash-dotted lines. Curves in reciprocal space marking k-points (black dots) at which bands in the surface electronic structure occur at energies (b) 0.006 eV and (c) -0.013 eV, obtained from the density of states projected onto surface atoms of the semi-infinite slab. K_x and K_y are two mutually perpendicular axes on the 2D BZ.	141

5.4	(a) Structural unit of AFM- \perp state of DyPdBi with magnetic moments (spins of Dy) oriented perpendicular to [111] axis. Its electronic structure (b) calculated along high symmetry lines shows an apparent gapped bulk state, while that along lines of low-symmetry reveals Weyl points (c). Locations of these four Weyl points are indicated as dots in the BZ (d). Red and black coloured dots denote Weyl points of +1 and -1 chirality.	143
5.5	Total and orbital projected band structure of AFM- \perp showing combined contributions of s , p and d orbitals of Dy, Pd and Bi atoms to bands near the gap or Weyl points.	144
5.6	Electronic structure of Dy-terminated (100) surface of AFM- \perp DyPdBi calculated using Wannier functions based tight-binding model with Wannier90 and WannierTools packages, displayed as contourplots of k -resolved density of states (a) in which the nodal points and conical band structural features are evident. Fermi arcs (b), the curves in reciprocal space marking k -points at which bands in the surface electronic structure occur at energies 0.004 eV obtained from the density of states projected onto surface atoms of the semi-infinite slab.	145
5.7	Origin of intrinsic AHC in the (a) triple point semimetallic AFM- \parallel and (b) Weyl semimetallic AFM- \perp phases of DyPdBi. The top left panels show electronic bands through the topologically protected nodes along with their spin character. The top right panels show anomalous Hall conductivity as function of energy. The bottom panels show Berry curvature $\Omega_{\alpha\beta}(k)$ along $Z' - \Gamma - Z$, summed over the occupied bands. σ_{AHC} and Ω have been obtained with Wannier90 and WannierBerri packages.	147
A.1	Equilibrium lattice parameters calculated as the average of 8 predictions. The experimental lattice parameters are obtained from [176].	159
A.2	Single crystal elastic moduli C_{11} (a), C_{12} (b) and C_{44} (c).	162
A.3	(a) Distribution of A , the universal measure of anisotropy in Re-PdBi. (b) Directional dependence of Young's modulus and shear modulus in anisotropic ScPdBi, LaPdBi and isotropic NdPdBi.	163
A.4	VRH approximation of polycrystalline elastic parameters: (a) bulk modulus (b) shear modulus (c) Young's modulus and (d) Poisson's ratio.	164
A.5	(a) Lamé's first parameter and measures of ductility as (b) Pugh ratio and (c) Cauchy pressure as estimated from VRH approximations of polycrystalline elastic parameters.	169
A.6	Speed of sound wave in Re-PdBi in (a) tension-compression mode (b) shear mode and (c) as average. (d) Debye temperatures of Re-PdBi. Experimental values of speed of sound are obtained from [232, 233]	171

B.1	$k.p$ perturbative model of quartic degree fitted to first principles results obtained for triple point (a) and Weyl (b) phases on $k_x = k_y = k_z = k$ lines for range $k = [-0.3, 0.3]$. Solid lines show DFT obtained bands whereas dashed lines show the fitted model.	183
C.1	(a) Semi-infinite slab made by stacking primitive magnetic unit cells along (100). Purple, light blue and yellow colors representing bismuth, dysprosium and palladium atoms respectively. The structure can have two terminations with lower surface being bismuth-terminated and top one being dysprosium terminated. (b-c) Surface states showing Fermi arc connectivity under different atomic termination in the triple point (TP) phase. (d-e) Fermi arc connectivity under different atomic termination in the Weyl phase.	192
C.2	(a) Semi-infinite slab made by stacking primitive magnetic unit cells along (100) of cubic conventional cell with purple, light blue and yellow colors representing bismuth, dysprosium and palladium atoms respectively. The structure can have two terminations with lower surface being bismuth-dysprosium-terminated and top one being palladium terminated. (b-c) Surface states showing Fermi arc connectivity under different atomic termination in the triple point (TP) phase. (d-e) Fermi arc connectivity under different atomic termination in the Weyl phase.	193
D.1	Equilibrium lattice parameters obtained using the antiferromagnetic unit cells as for (a) $a_{\text{ErPdBi}} = 6.6951\text{\AA}$ and (b) $a_{\text{GdPdBi}} = 6.7780\text{\AA}$. . .	196
D.2	Calculated Hubbard U parameters of (a) $U_{\text{ErPdBi}}^f = 7.733\text{eV}$ and (b) $U_{\text{GdPdBi}}^f = 5.942\text{eV}$	197
D.3	Variation of total energy as a function of parameters (θ, ϕ) for (a) ErPdBi and (b) GdPdBi.	197

List of Tables

1.1	Topological classes of hermitian Hamiltonian matrices and their materials realization.	9
1.2	Space groups hosting triple points. Adapted from [39].	22
1.3	Milestones in topological research in RE-half Heusler alloys	40
3.1	Flatband sublattices obtained from Fig.3.5	83
3.2	New monolayer flatband sublattices identified from Fig 3.6	88
3.3	New bilayer flatband sublattices identified from Fig 3.6	89
3.4	New multilayer flatband sublattices identified from Fig 3.6	90
4.1	Number and momenta of triple points in YPdBi for different values of tensile strain	120
5.1	Locations (k , ϵ) of nodes of crossing of linearly dispersed bands, the triple and Weyl points, in DyPdBi. ΔE represents their energies in eV with respect to the Fermi energy.	139
B.1	Fitting parameters obtained for triple point and Weyl phase.	185

Abbreviations

AI	A rtificial I ntelligence
ML	M achine L earning
MD	M olecular D ynamics
DFT	D ensity F unctional T heory
AFM	A nti F erro M agnet
TKNN	T ouless- K ohmoto- N ightingale-den N ijs
TRIM	T ime R eversal I nvariant M omenta
BZ	B rillouin Z one
SOC	S pin O rbital C oupling
QSH	Q uantum S pin H all
TI	T opological I nsulator
TCI	T opological C rystalline I nsulator
FCC	F ace C entered C ubic
MATBG	M agic- A ngle T wisted B ilayer G raphene
IC	I ntegrated C ircuit
MOSFET	M etal O xide S ilicon F ield E ffect T ransistors
SOT	S pin- O rbital T orque
NOMAD	N Ovel M aterials D iscovery
OQMD	O pen Q uantum M aterials D atabase
AFLOW	A utomat I c F LOW for M aterials D iscovery
C2DB	C omputational 2D M aterials D ata B ase
RE	R are E arth
SDH	S ubhnikov de H aas
AHC	A nomalous H all C onductivity
AHE	A nomalous H all E ffect
KS	K ohn- S ham

HDBSCAN	H ierarchical D ensity- B ased S patial C lustering of A pplications with N oise
CNN	C onvolutional N eural N etwork
t-SNE	t -distributed S tochastic N eighbourhood E mbedding
DOS	D ensity of S tates
DBCV	D ensity- B ased C lustering V alidation
GGA	G eneralized G radient A pproximation
LDA	L ocal-density approximation
DMFT	D ynamical mean-field theory
PBE	P erdew- B urke- E rnzerhof
HSE	H eyd- S cuseria- E rnzerhof
MBJ	modified B ecke- J ohnson
SCAN	S trongly constrained and appropriately normed
SOAP	S mooth O verlap of A tomistic P ositions
MBTR	M any-body T ensor R epresentation
LoStOP	L ocal S tructure O rders P arameters
LLE	L ocally L inear E mbedding
UMAP	U niform M anifold A pproximation
RBIS	relative band inversion strength
MLWF	M aximally- L ocalized W annier F unction
VASP	V ienna A b-initio S imulation P ackage
QE	Q uantum E spresso
ARPES	angle-resolved photoemission spectroscopy
SCF	self-consistent field
NSCF	non-self-consistent field
ONCV	O ptimized N orm- C onserving V anderbilt